Abayomi S. Oke, Winifred N. Mutuku, Mark Kimathi, and Isaac L. Animasaun*

Insight into the dynamics of non-Newtonian Casson fluid over a rotating non-uniform surface subject to Coriolis force

https://doi.org/10.1515/nleng-2020-0025
Received Jun 14, 2020; accepted Aug 31, 2020.

Abstract: Casson fluid model is the most accurate mathematical expression for investigating the dynamics of fluids with non-zero plastic dynamic viscosity like that of blood. Despite huge number of published articles on the transport phenomenon, there is no report on the increasing effects of the Coriolis force. This report presents the significance of increasing not only the Coriolis force and reducing plastic dynamic viscosity, but also the Prandtl number and buoyancy forces on the motion of non-Newtonian Casson fluid over the rotating non-uniform surface. The relevant body forces are derived and incorporated into the Navier-Stokes equations to obtain appropriate equations for the flow of Newtonian Casson fluid under the action of Coriolis force. The governing equations are non-dimensionalized using Blasius similarity variables to reduce the nonlinear partial differential equations to nonlinear ordinary differential equations. The resulting system of nonlinear ordinary differential equations is solved using the Runge-Kutta-Gills method with the Shooting technique, and the results depicted graphically. An increase in Coriolis force and non-Newtonian parameter decreases the velocity profile in the x–direction, causes a dual effect on the shear stress, increases the temperature profiles, and increases the velocity profile in the z–direction.

Keywords: Coriolis force; Buoyancy-Induced flow; Casson fluid; Rotating non-uniform surface

Abayomi S. Oke, Department of Mathematics and Actuarial Science, Kenyatta University, Kenya
Department of Mathematical Sciences, Adekunle Ajasin University, Akungba Akoko, Nigeria, E-mail: okeabayomisamuel@gmail.com
Winifred N. Mutuku, Department of Mathematics and Actuarial Science, Kenyatta University, Kenya,
E-mail: mutukuwinnie@gmail.com
Mark Kimathi, Department of Mathematics and Actuarial Science, Machakos University, Kenya, E-mail: memkimathi@gmail.com
***Corresponding Author: Isaac L. Animasaun,** Department of Mathematical Sciences, Federal University of Technology Akure, PMB 704, Nigeria, E-mail: ilanimasaun@futa.edu.ng

Highlights

- Dynamics of non-Newtonian Casson fluid over a surface with non-uniform thickness is investigated.
- The significance of increasing Coriolis force on the dynamics of non-Newtonian Casson fluid is explored.
- Primary velocity decreases with Prandtl number, Casson fluid parameter, and Coriolis force but secondary velocity responds oppositely to the parameters.
- Coriolis force and the Casson fluid parameter have similar effects on Casson fluid flow over a rotating surface with non-uniform thickness.
- Simultaneously increasing Coriolis force, Casson fluid parameter and Prandtl number reduces the primary skin friction coefficient and heat transfer rate but increases the secondary skin friction coefficient.

1 Introduction

The centrifugal force (acting radially outward from the axis of rotation), the Azimuthal force (parallel but opposite to the velocity, also known as the Euler force), and the Coriolis force (outward and perpendicular to angular velocity) are the three forces experienced in a rotating frame of reference; Debnath [1]. These forces are fictitious since they are not generated from interaction with any external body but are responsible to keep the motion rotational. Coriolis force is the fictitious force responsible for the deflection of the trajectory of a moving object in a rotating frame; Deng et al. [2] and Archana et al. [3]. The Coriolis effect is responsible for many natural occurrences such as the direction of the cyclones, organization of the magnetic columns and electric properties of the Earth, hydromagnetic flow of the earth's liquid contents etc. The Coriolis force is also very significant in the flow equations, just as other inertial and viscous forces and of magnitude comparable with other magnetohydrodynamic forces; Shiferaw et al. [4].

Common surfaces on which flows are considered to include the horizontal surface, vertical surface, inclined surface etc. Some authors have considered flow over vertical cones, and wedges; Takhar et al. [5], Ghalambaz et al. [6] and Makinde and Animasaun [7, 8]. Meanwhile, fluid flow over surfaces whose thickness is non-uniform is common in nature and other physical applications. For instance, a bullet spins about its axis through the air as it is fired, the air heated by the sun touches and flows over the Earth rotating surface, a traveling missile in space etc. These surfaces are not flat plates or inclined planes cylinders whose thickness is uniform throughout but they possess surface with variable thickness. A way to generalize such surfaces with non-uniform thickness is to consider the upper horizontal surface of a paraboloid of revolution as suggested by Animasaun [9]. Due to the appearance of surfaces with non-uniform thickness in many natural occurrences and many physical applications, researchers have turned attention to not only examine but also explore transport phenomena over an upper horizontal surface of a paraboloid of revolution; Animasaun [10], Liu et al. [11], Koriko et al. [12], Makinde et al. [13], and Ajayi et al. [14].

Fluids that do not obey Newton's viscosity law are regarded as non-Newtonian fluids. The nature of these non-Newtonian fluids cannot be captured into a single model and these lead to different proposals for different fluid behaviors. Casson fluid model is one of the non-Newtonian fluids which models fluids such as jelly, honey, fruit juices, soup, and blood etc. Casson fluid is a shear-thinning fluid exhibiting yield stress and which has infinite viscosity at a low shear rate and zero viscosity at the infinity shear rate; RamReddy et al. [15] and Amanulla et al. [16]. In other words, Casson fluid behaves like a solid when yield stress is more than the shear stress but behaves like a liquid and flows when the yield stress is less than the shear stress. Certain categories of ink and blood are examples of Casson fluid. Blood obeys Newtonian law at high shear stress through larger arteries but becomes non-Newtonian at low shear stress through smaller arteries; see Batra and Jena [17], Siddiqui et al. [18], Abegunrin et al. [19], Sankar and Lee [20], Mukhopadhyay et al. [21], Pramanik [22], Animasaun [23], Kataria and Patel [24], and Zaib et al. [25].

Sequel to the fact that Casson fluid model is in close agreement with the rheology of blood, Abbasian et al. [26] used different blood viscosity models to simulate the behavior of blood. Models used include Bingham, Carreau, Casson, modified Casson, Cross, Kuang-Luo (K-L), Powell-Erying, Power-law, and Walburn-Schneck models and the results show that the time-averaged velocity at the center of the arteries produced in the CFD simulations that uses the Carreau, modified Casson or Quemada blood viscosity models corresponded exceptionally well with the clinical measurements regardless of stenosis severities and hence, highlights the usefulness of these models to determine the potential determinants of blood vessel wall integrity such as dynamic blood viscosity, blood velocity, and wall shear stress. Dubey et al. [27] presented a two-dimensional theoretical study of hemodynamics through a diseased permeable artery with mild stenosis and an aneurysm present. The two models adopted to mimic non-Newtonian characteristics of the blood flow are the Casson (in the core region) and the Sisko (in the peripheral region). It is observed that by increasing the thermal buoyancy parameter, i.e. Grashof number (G_r), the nanoparticle concentration and temperature decrease and it was remarked that simulations are relevant to transport phenomena in pharmacology and nano-drug targeted delivery in hematology.

Recently, Koriko [28] explored the effect of Coriolis force on the flow of Newtonian fluid over a rotating surface with non-uniform thickness. It was observed that the horizontal and vertical velocities reduce with a combined increase in shear stress and Coriolis force whereas the buoyancy force has an increasing effect on the overall velocity and temperature distribution of the flow. The present study is an extension of Ref. [28] to a non-Newtonian Casson fluid. But, so far no attempt has been made to investigate the effect of Coriolis force on the flow of Casson fluid over a surface with non-uniform thickness whose importance cannot be overlooked in energy production, nuclear reactor cooling, biomedical applications, etc. Such a study is important in the design of turbines and turbo-machines, in estimating the flight path of rotating wheels and spin, stabilized missiles, and in the modeling of many geophysical vortices. A typical example of Casson fluid flow over a nonuniform surface under the action of Coriolis force can be practically observed in a bioreactor, in which a microorganism-carrying fluid flows in a tunnel with a non-uniform surface.

This present study investigates the influence of Coriolis force on the properties of Casson fluid flow across surfaces with non-uniform thickness. The research questions for the investigation are

1. What is the significance of Coriolis force on the flow of Casson fluid over a rotating surface with non-uniform thickness?

2. What is the combined effect of Casson fluid parameter and Coriolis force on the flow of Casson fluid over a rotating surface with non-uniform thickness?
3. What is the combined effect Coriolis force and Prandtl number on the flow of Casson fluid over a rotating surface with non-uniform thickness?
4. How does Coriolis force affect the Skin Friction in both x– and y–directions and the heat transfer rate?

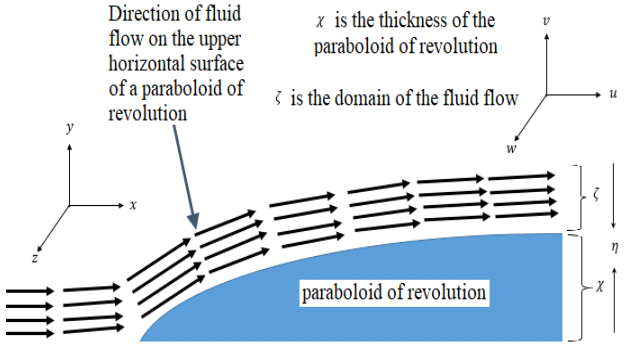

Figure 1: Physical Configuration in xy-domain

2 Mathematical Formulation of Governing Equations

Consider a steady boundary layer flow of Casson fluid over the upper surface of a horizontally stretching surface of paraboloid of revolution where the fluid is in a rigid body rotation with the surface about the y– axis. The surface rotates with a uniform angular velocity $\boldsymbol{\Omega}$ while it is heated and stretched linearly with velocity $u = U_0 (x+b)^m$. The flow is over the non-uniform region $y = A (x+b)^{\frac{1-m}{2}}$, where m is the velocity index and A and b is some arbitrary constants related to the thickness of the object. As shown in Fig. (1), Coriolis force is produced in the rotating system as the fluid flows. According to Mustafa *et al.* [29], the rheological equation of an isotropic and incompressible flow of a Casson fluid can be written as

$$\tau_{ij} = \begin{cases} 2\left(\mu + \frac{p_y}{\sqrt{2\pi}}\right) e_{ij} & \pi > \pi_c \\ 2\left(\mu + \frac{p_y}{\sqrt{2\pi_c}}\right) e_{ij} & \pi < \pi_c \end{cases}$$

where p_y is known as yield stress of the fluid expressed as

$$p_y = \frac{\mu_b \sqrt{2\pi}}{\beta^*},$$

μ is known as the plastic dynamic viscosity of the non-Newtonian fluid, π is the product of the component of deformation rate with itself $(\text{i.e. } \pi = e_{ij}e_{ij})$, e_{ij} is the (i,j)th component of the deformation rate and $\pi_c$is the critical value based on the non-Newtonian model. For Casson fluid, where $\pi > \pi_c$, we have the dynamic viscosity given as

$$\mu^* = \mu + \frac{p_y}{\sqrt{2\pi}} = \mu\left(1 + \frac{1}{\beta^*}\right)$$

Following Ref. [28], the body forces comprise of Coriolis force and buoyancy force are

$$f_{bx} = \left(\frac{m+1}{2}\right) g\beta(T - T_\infty) - 2\frac{\Omega\aleph w}{U_0(x+b)^{2-m}}, \tag{1}$$

$$f_{bz} = \left(\frac{m+1}{2}\right) g\beta(T - T_\infty) + 2\frac{\Omega\aleph u}{U_0(x+b)^{2-m}}. \tag{2}$$

The boundary layer equations governing the flow of non-Newtonian Casson fluid over the upper horizontal surface of a paraboloid of revolution under the influence of Coriolis force is therefore given as the system of nonlinear partial differential equations

$$\frac{\partial u}{\partial x} + \frac{\partial v}{\partial y} = 0 \tag{3}$$

$$u\frac{\partial u}{\partial x} + v\frac{\partial u}{\partial y} + 2\frac{\Omega\aleph w}{U_0(1+x)^{2-m}} = \frac{\mu}{\rho}\left(1 + \frac{1}{\beta^*}\right)\frac{\partial^2 u}{\partial y^2} + \left(\frac{m+1}{2}\right) g\beta(T - T_\infty) \tag{4}$$

$$u\frac{\partial w}{\partial x} + v\frac{\partial w}{\partial y} - 2\frac{\Omega\aleph u}{U_0(1+x)^{2-m}} = \frac{\mu}{\rho}\left(1 + \frac{1}{\beta^*}\right)\frac{\partial^2 w}{\partial y^2} + \left(\frac{m+1}{2}\right) g\beta(T - T_\infty) \tag{5}$$

$$u\frac{\partial T}{\partial x} + v\frac{\partial T}{\partial y} = \frac{\kappa}{\rho c_p}\frac{\partial^2 T}{\partial y^2}. \tag{6}$$

subject to the boundary conditions

$$u = U_0(x+b)^m, \quad v = 0, \quad w = 0, \quad T = T_w(x) \quad at \quad y = A(x+b)^{\frac{1-m}{2}} \tag{7}$$

$$u \to 0, \quad w \to 0, \quad T \to T_\infty \quad as \quad y \to \infty \tag{8}$$

The quantities of interest are the Nusselt number proportional to the heat transfer, the skin friction of the flow along x–direction and z–direction defined as

$$C_{fx} = \frac{\tau_{wx}}{\rho\sqrt{\frac{m+1}{2}}U_w^2}, \quad C_{fz} = \frac{\tau_{wz}}{\rho\sqrt{\frac{m+1}{2}}U_w^2},$$

$$\text{and} \quad N_{ux} = \frac{(x+b)\,q_w}{\kappa\,(T_w - T_\infty)\sqrt{\frac{m+1}{2}}}. \tag{9}$$

In the Equation (9), τ_w is the shear stress (skin friction) along the upper horizontal surface of a paraboloid of revolution defined as

$$\tau_{wx} = \mu\left(1+\frac{1}{\beta}\right)\left.\frac{\partial u}{\partial y}\right|_{y=A(x+b)^{\frac{1-m}{2}}}$$
$$\text{and} \quad \tau_{wz} = \mu\left(1+\frac{1}{\beta}\right)\left.\frac{\partial w}{\partial y}\right|_{y=A(x+b)^{\frac{1-m}{2}}} \tag{10}$$

and the heat flux q_w at the wall is defined as

$$q_w = -\kappa\left.\frac{\partial T}{\partial y}\right|_{y=A(x+b)^{\frac{1-m}{2}}}. \tag{11}$$

The dimensional governing equations above were reduced to dimensionless equations by using the similarity variables below and the conversion domain $\zeta = \eta + \chi$ (i.e. $\eta = \zeta - \chi$) capable to transform the domain from $\zeta \in [\chi, \infty]$ to $\eta \in [0, \infty]$.

$$\zeta = y\left(\frac{m+1}{2}\frac{U_0}{\vartheta}\right)^{\frac{1}{2}}(x+b)^{\frac{m-1}{2}}, \quad u(x,y) = \frac{\partial \psi}{\partial y},$$
$$\Theta(\eta) = \frac{T - T_\infty}{T_w - T_\infty}, \quad v(x,y) = -\frac{\partial \psi}{\partial x},$$
$$\psi = \left(\frac{2}{m+1}\right)^{1/2}(\vartheta U_o)^{1/2}(x+b)^{\frac{m+1}{2}}F(\eta),$$
$$w(x,y) = U_0\,(x+b)^m\,H(\eta). \tag{12}$$

The dimensionless equations are of the form

$$\left(1+\frac{1}{\beta^\star}\right)F''' + F''F - \frac{2m}{m+1}F'F' - \frac{K}{m+1}H + Gr\Theta = 0, \tag{13}$$

$$\left(1+\frac{1}{\beta^\star}\right)H'' + H'F - \frac{2m}{m+1}HF' + \frac{K}{m+1}F' + Gr\Theta = 0, \tag{14}$$

$$\Theta'' + PrF\Theta' - Pr\left(\frac{1-m}{m+1}\right)F'\Theta = 0. \tag{15}$$

with the boundary conditions

$$F' = 1, \quad F = \left(\frac{1-m}{m+1}\right)\chi, \quad H = 0, \quad \Theta = 1 \quad at \quad \eta = 0 \tag{16}$$

$$F' \to 0, \quad H \to 0, \quad \Theta \to 0 \quad as \quad \eta \to \infty. \tag{17}$$

Whereas the dimensionless boundary conditions are

$$K = \frac{4\Omega\aleph}{U_0^2(x+b)}, \quad Gr = \frac{g\beta\,(T_w - T_\infty)}{U_0^2\,(x+b)^{2m-1}}, \quad Pr = \frac{\rho c_P \vartheta}{\kappa},$$
$$\chi = A\left(\frac{m+1}{2}\frac{U_0}{\vartheta}\right)^{\frac{1}{2}}. \tag{18}$$

are the rotational parameter, Grashof number, Prandtl number and the thickness parameter respectively. The skin frictions along the x–direction and z–direction become

$$Re_x^{\frac{1}{2}}C_{fx} = F''(0) \quad \text{and} \quad Re_x^{\frac{1}{2}}C_{fz} = H'(0).$$

respectively and the heat transfer coefficient becomes

$$Re_x^{-\frac{1}{2}}N_{ux} = -\Theta'(0).$$

3 Numerical Procedure

In order to obtain the numerical solution of the aforementioned dimensionless governing equation, it is necessary to break it down into a system of first order ordinary differential equations

$$Y_1' = Y_2,$$
$$Y_2' = Y_3,$$
$$Y_3' = \left(1+\frac{1}{\beta^\star}\right)^{-1}\left(-Y_3Y_1 + \frac{2m}{m+1}Y_2^2 + \frac{K}{m+1}Y_4 - GrY_6\right),$$
$$Y_4' = Y_5,$$
$$Y_5' = \left(1+\frac{1}{\beta^\star}\right)^{-1}\left(Y_5Y_1 - \frac{2m}{m+1}Y_4Y_2 + \frac{K}{m+1}Y_2 + GrY_6\right),$$
$$Y_6' = Y_7,$$
$$Y_7' = PrY_1Y_7 - Pr\left(\frac{1-m}{m+1}\right)Y_2Y_6,$$

where

$$Y_1 = f, \; Y_2 = f', \; Y_3 = f'', \; Y_4 = h, \; Y_5 = h', \; Y_6 = \theta, \; Y_7 = \theta'.$$

with the initial conditions

$$Y_1(0) = \left(\frac{1-m}{m+1}\right)\chi, \; Y_2(0) = 1, \; Y_4(0) = 0, \; Y_6(0) = 1$$
$$Y_3(0) = s_1, \; Y_5(0) = s_2, \; Y_7(0) = s_3.$$

where s_1, s_2, s_3 are obtained using the shooting technique, and the system is solved numerically using the Runge-Kutta-Gills method (for some other methods of solution, see [30]). The system is solved using a step size $\Delta\eta = 0.01$ and absolute tolerance 10^{-6}. The results obtained are displayed as graphs and the effect of Coriolis force is investigated while the pertinent parameters increase. The flow becomes Newtonian as $\beta \to \infty$ and the surface becomes a horizontal plane as $m \to 1$ and hence this report is validated by comparing the results as $\beta \to 0$ and as $m \to 1$.

4 Analysis of Results and Discussion

In this section, the effect of increasing rotation parameter alongside some other pertinent parameters is illustrated in the given graphs. It is important to reiterate here that an increase in the rotation parameter consequently implies an increase in Coriolis force. The results are validated by comparing the skin friction coefficient and Nusselt number as $\beta^* \to \infty$ with the result of [28] in Table (1) and there is a good agreement. It is worth noting that the surface becomes a flat surface as $m \to 1$. Table (2) shows that the skin friction coefficient in all directions increases as the surface becomes flat horizontal plane $m \to 1$ with increasing K whereas the Nusselt number decreases as $m \to 1$ and K increases.

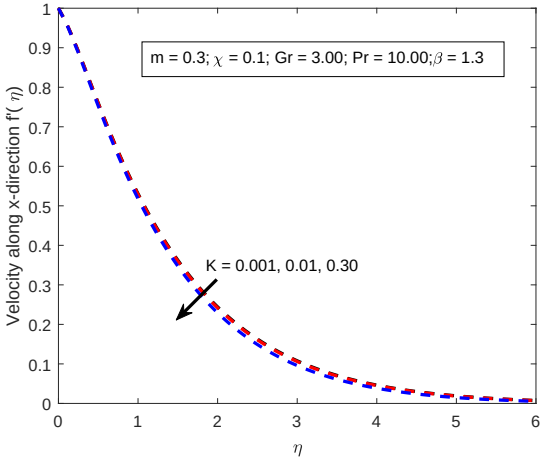

Figure 2: Variation of velocity in the x–direction with rotation parameter

4.1 Significance of increasing Coriolis force

Coriolis force is directly proportional to the rotation of the surface. The impact of increasing rotation of the surface with non-uniform thickness is explored on the Casson fluid flows. When $Gr = 3.0$, $Pr = 10$, $m = 0.3$, $\chi = 0.1$ and $\beta = 1.3$, the rotation parameter was varied to study its effect on the dynamics of the flow. The velocity in the x–direction, as shown in Fig. (2) decreases as rotation increases. A closer view of Fig. (2) for $1.68 \leq \zeta \leq 1.95$ is illustrated as Fig. (3)). Meanwhile, Fig. (4) shows that the velocity in the z–direction increases as rotation increases.

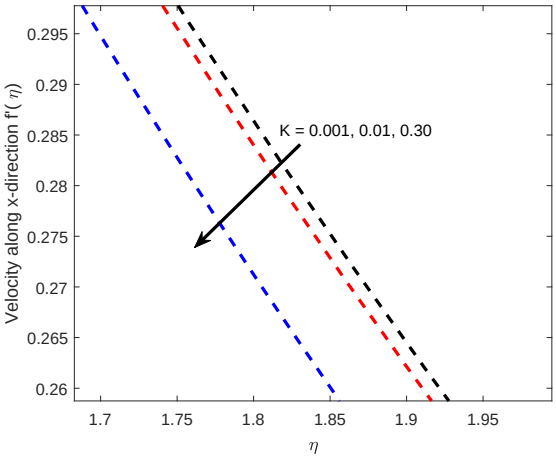

Figure 3: A zoomed portion of Fig. (2)

This can be traced to the fact that the surface is rotated counterclockwise thereby enhancing the velocity in the z–direction while reducing the velocity in the x–direction. It is worth noting that the presence of rotation in the flow is responsible for the dual nature of the shear stress of the flow as depicted in Fig. (5). From Fig. (6), it is shown that increasing rotation indeed causes a reduction in the shear stress within the boundary layer near the rotating surface while Fig. (7) shows that increasing rotation causes a rise in the shear stress across the fluid layers near the free stream. More so, the minimum shear stress at the boundary layer is obtained at high rotation. Fig. (8) shows that increasing rotation leads to an increase in the temperature profile. Fig. (9) shows a closer view of the results presented as Fig. (9) for $0.2925 \leq \zeta \leq 0.2945$. This can be traced to the fact that an increase in the rotation causes a conversion of a portion of the internal energy into heat energy which in turn raises the overall temperature of the flow.

4.2 Significance of decreasing plastic dynamic viscosity

The effect of Casson fluid parameter β on the flow of Casson fluid over a rotating upper horizontal surface of a paraboloid of revolution is explored. The pertinent parameters are fixed as $Gr = 3.0, Pr = 10, m = 0.3$ and $\chi = 0.25$ while β is varied. It is important to take note that as $\beta \to \infty$, the fluid reduces to Newtonian. Fig. (10) reveals that the simultaneous increase in both Casson fluid parameter and rotation parameter has retarding effects on the velocity in the x–direction. As Casson fluid parameter increases simultaneously with the rotation parameter, it is found that the behaviour of the velocity profiles in

Table 1: Comparison of results for validation as $\beta^* = 100000$.

K	$f''(0)$		$h'(0)$		$-\theta'(0)$	
	Present	Ref. [28]	Present	Ref. [28]	Present	Ref. [28]
0	-0.314750	-0.314750	0.615684	0.615690	3.439016	3.439016
0.1	-0.320717	-0.320717	0.672564	0.672570	3.437632	3.437631
0.2	-0.329661	-0.329661	0.728999	0.729006	3.435503	3.435503
0.3	-0.341460	-0.341460	0.784459	0.784466	3.432659	3.432659
0.4	-0.355892	-0.355892	0.838427	0.838434	3.429142	3.429141
0.5	-0.372634	-0.372634	0.890443	0.890451	3.425021	3.425021

Table 2: Results for increasing K as the surface becomes a flat horizontal surface

$K = 0.00$				$K = 0.10$				$K = 0.20$			
m	C_{fx}	C_{fz}	N_{ux}	m	C_{fx}	C_{fz}	N_{ux}	m	C_{fx}	C_{fz}	N_{ux}
0	0.27926	0.52938	4.52207	0	0.28780	0.61032	4.52019	0	0.30283	0.68967	4.51681
0.2	0.30856	0.58872	3.74588	0.2	0.31514	0.65183	3.74436	0.2	0.32547	0.71429	3.74195
0.4	0.31753	0.64108	3.17135	0.4	0.32303	0.69286	3.17006	0.4	0.33093	0.74434	3.16816
0.6	0.31648	0.68769	2.72531	0.6	0.32129	0.73164	2.72417	0.6	0.32777	0.77545	2.72259
0.8	0.31020	0.72950	2.36668	0.8	0.31453	0.76772	2.36567	0.8	0.32007	0.80588	2.36428
1	0.30114	0.76725	2.07046	1	0.30511	0.80110	2.06951	1	0.30999	0.83494	2.06832

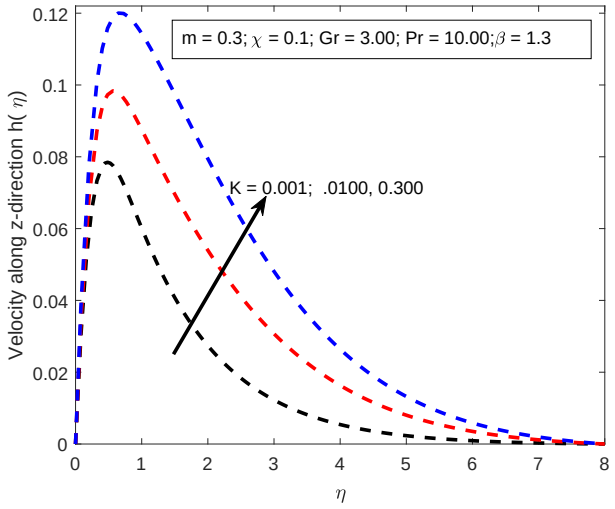

Figure 4: Variation of velocity profiles in the z-direction profile with rotation parameter

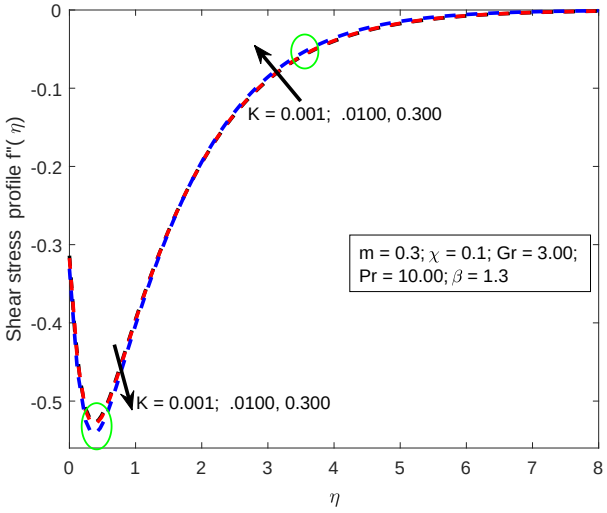

Figure 5: Variation of shear stress profile with rotation parameter

the z–direction is separated. Fig. (11) reveals that at low rotation ($K = 0.001$), increasing Casson fluid parameter causes an increase in velocity profile in the z–direction. Meanwhile, as the rotation parameter increases, there is a dual effect of Casson fluid parameter on the velocity profile in the z–direction. The results corroborates with the results of Malik *et al.* [31] and Patel [32]. Thus, at high rotation, the velocity profile in the z–direction experiences an increase at the boundary layer but a decrease at the free stream; see Fig. (11). Fig. (12) shows the effect of the rotation parameter on the shear stress. There is a dual effect of rotation parameter on the shear stress; an increase in the rotation parameter leads to a decrease in shear stress at the boundary layer but an increase in the shear stress at the free stream. The shear stress reaches the minimum in the boundary layer when the rotation is moderately high. Increasing Casson fluid parameter implies decreasing yield stress and the fluid behaves as Newtonian fluid as Casson parameter becomes large, reducing the boundary layer thickness. This leads to a reduction in the shear stress as the flow becomes Newtonian (i.e. $\beta \to \infty$); see Fig. (13). Fig. (14) shows that an increase in the rotation parameter

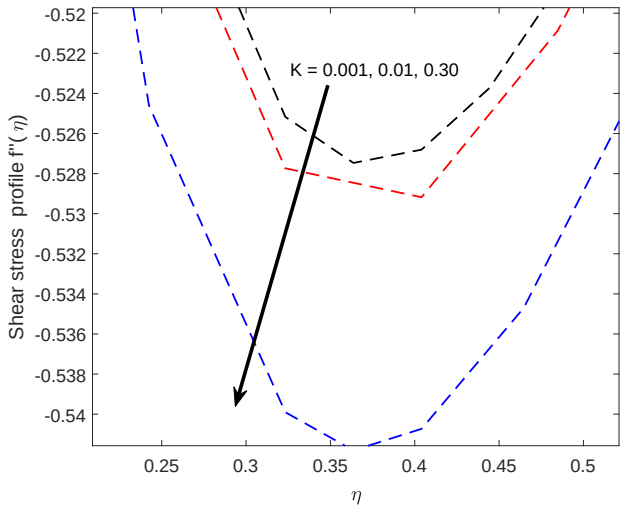

Figure 6: A zoomed portion of the boundary layer of Fig.(5)

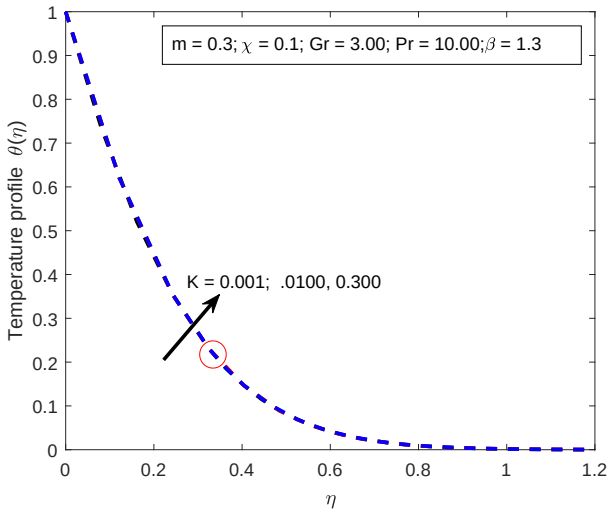

Figure 8: Variation of temperature profile with rotation parameter

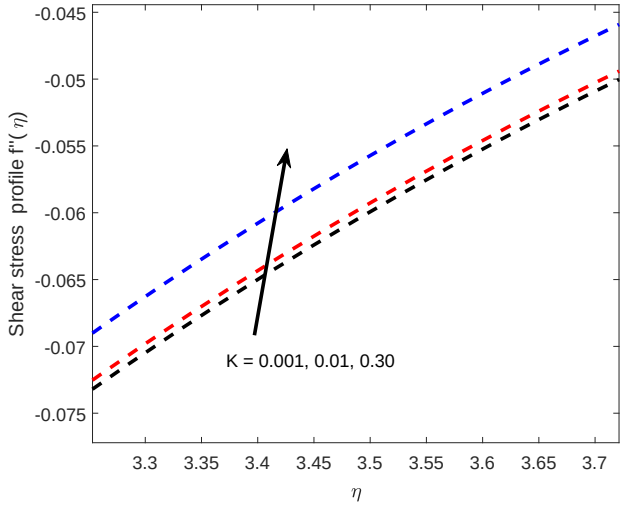

Figure 7: A zoomed portion of the free stream of Fig.(5)

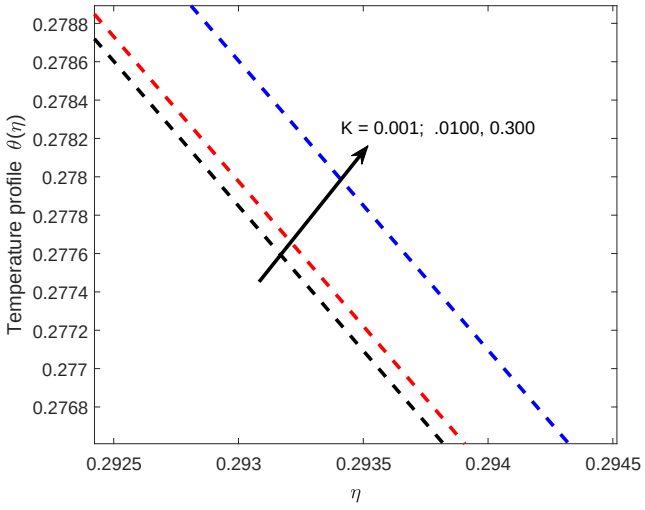

Figure 9: A zoomed portion of Fig. (8)

leads to a slight increase in the temperature profile. As further shown in Fig. (15), a simultaneous increase in both the Casson fluid parameter and rotation parameter leads to an increase in the temperature profiles.

4.3 Significance of increasing Prandtl number

In this section, the effects of Coriolis force as the Prandtl number increases for the flow of Casson fluid over the upper horizontal surface of the paraboloid of revolution are studied. Since Prandtl number is the ratio of the momentum diffusivity to the thermal diffusivity then an increase in the Prandtl number implies a decrease in the thermal diffusivity or increase in the momentum diffusivity. Consequently, as the Prandtl number increases, convection becomes more responsible for the transfer of energy than heat diffusion. The effects of Prandtl number was captured for $Gr = 3$, $m = 0.3$, $\chi = 0.25$, $\beta = 1.3$. Fig. (16) reveals that the simultaneous increase in both Prandtl number and rotation parameter has retarding effects on the velocity in the x–direction. Fig. (17) reveals that an increase in Prandtl number has retarding effects on the velocity in the z–direction but an increase in the rotation parameter tends to counter the retardation caused by the increase in the Prandtl number. Thus the peak of the velocity in the z-direction is obtained at high rotation and low Prandtl number. As thermal diffusivity reduces in a rotating system, the system expends some energy to

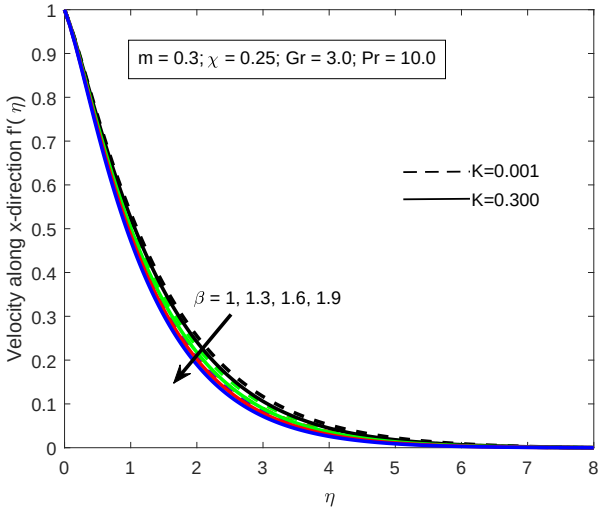

Figure 10: Variation of velocity profile in the x–direction with Casson fluid parameter

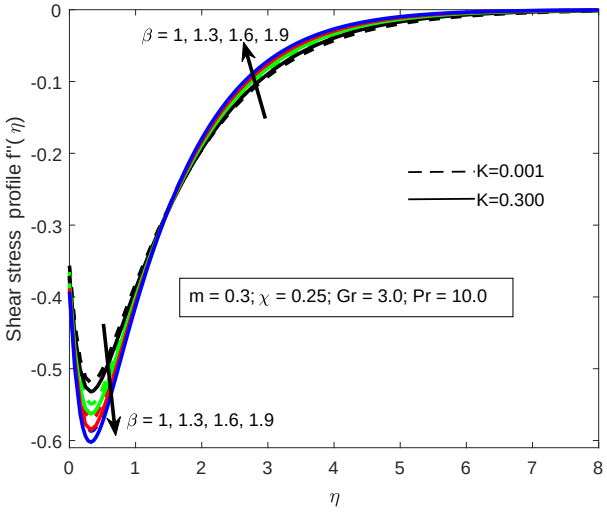

Figure 12: Variation of shear stress profile with small magnitudes of Casson fluid parameter

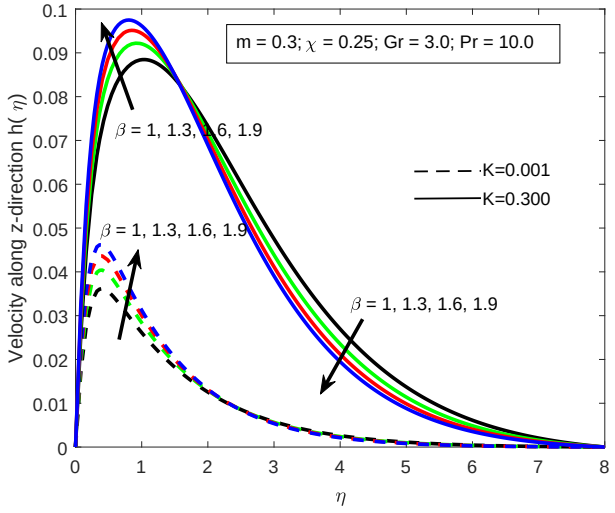

Figure 11: Variation of velocity profile in the z-direction with Casson fluid parameter

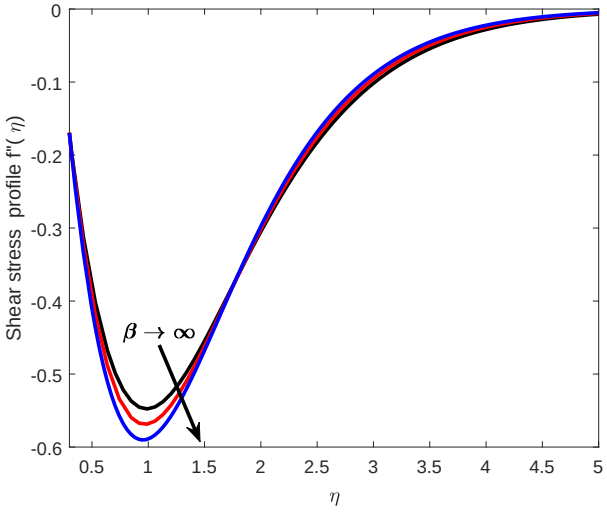

Figure 13: Variation of shear stress profile with large magnitudes of Casson fluid parameter

balance itself, hence it is practically expected that the velocity reduces generally.

As shown in Fig. (1), the surface rotates counterclockwise and this enhances the flow in the z–direction. This is confirmed by the finding in Fig. (17). This results is in agreement with the existing results of Malik *et al.* [31], Patel [32], Animasaun *et al.* [23], and Koriko *et al.* [28]. As shown in Fig. (18), a simultaneous increase in Prandtl number and rotation parameter has a dual effect on the shear stress such that the shear stress decreases close to the boundary layer but increases at the free stream. It is also pertinent to note that an increase in the rotation parameter further magnifies the effect of Prandtl number on the shear stress. The minimum shear stress at the boundary layer is obtained at high rotation and high Prandtl number while the minimum shear stress at the free stream is obtained at low rotation and low Prandtl number. The result is in agreement with the result of Koriko *et al.* [28]. An increase in Prandtl number has a retarding effect on the temperature profile as shown in Fig. (19). The minimum temperature profile is obtained at low rotation and high Prandtl number. As rotation increases, the effect of increasing Prandtl number tends to cancel out. It can be concluded that as long as the angular speed is within a certain range, the effect of increasing Prandtl number on the

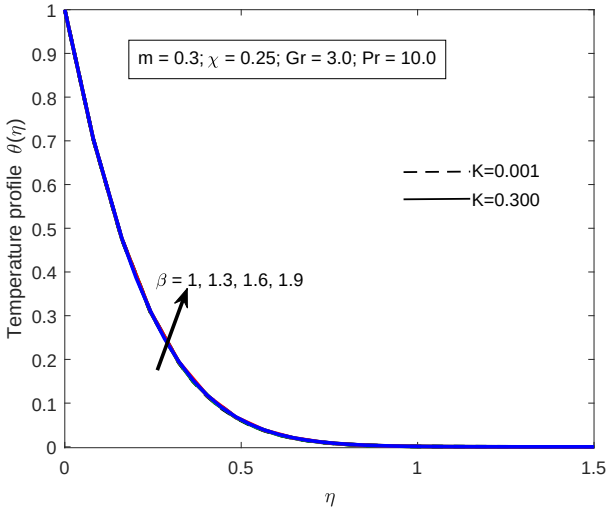

Figure 14: Variation of temperature profile with Casson fluid parameter

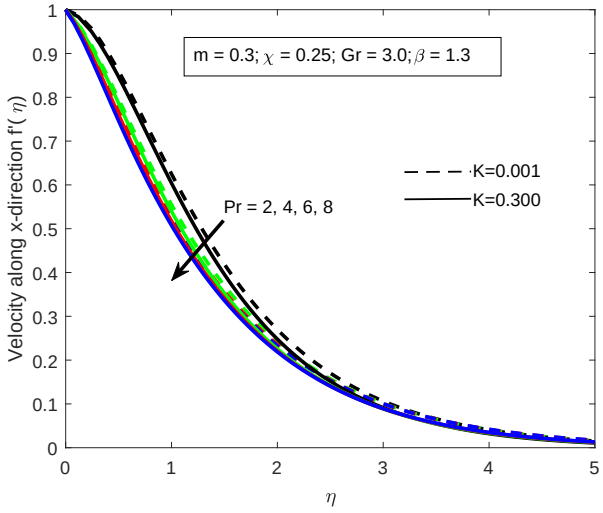

Figure 16: Variation of velocity profile in the x-direction with Prandtl number

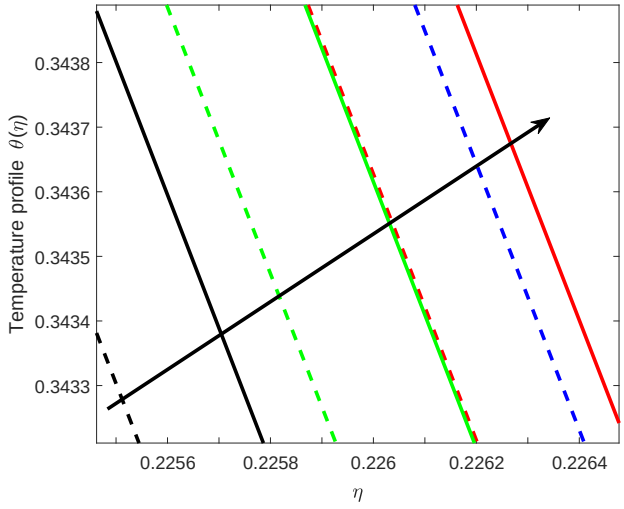

Figure 15: A zoomed portion of Fig. (??)

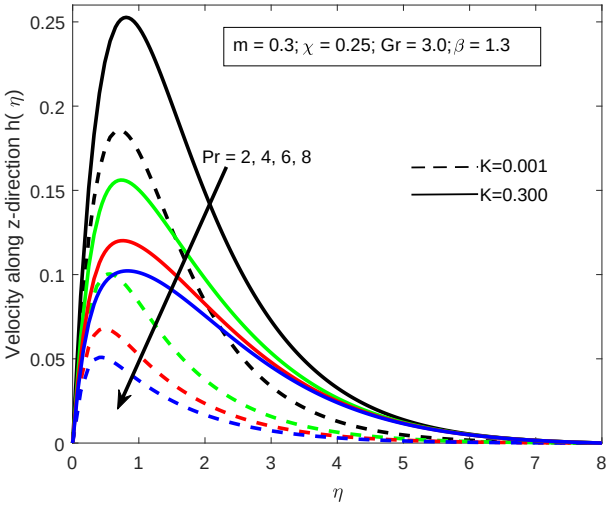

Figure 17: Variation of velocity profile in the z-direction with Prandtl number

flow of Casson fluid over a rotating surface with nonuniform thickness can be canceled by increasing rotational force.

4.4 Significance of increasing buoyancy forces

The dynamics of Casson fluid flow over a rotating surface with non-uniform thickness at various levels of buoyancy forces are outlined in this subsection. The parameter values are chosen as $Pr = 7.56$, $m = 0.3$, $\chi = 0.25$, $\beta = 1.3$. It is worth mentioning here that an increase in Grashof number, which is a consequence of an increase in temperature difference between wall temperature and free stream temperature, causes an increase in buoyancy. Fig. (20) and Fig. (21) show that the velocity in x–direction and the velocity in the z-direction increase with an increase in the buoyancy. However, as the rotation increases alongside an increase in the Grashof number, the velocity in the x-direction is affected negatively. Meanwhile, the velocity in the z-direction is positively affected. Hence, an increase in buoyancy increases the velocity in the x–direction and the velocity in the z-direction of the flow but increasing rotation, alongside an increase in the buoyancy, reduces the velocity in the x–direction while increasing the velocity in the z–direction. Clearly, as buoyancy increases, the sys-

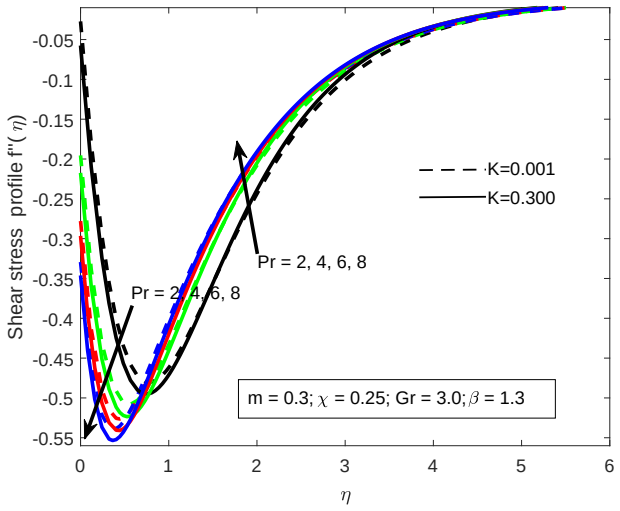

Figure 18: Variation in $F''(\eta)$ with P_r

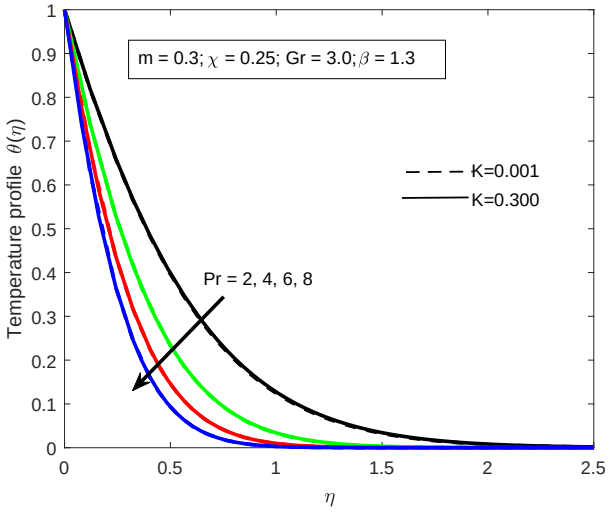

Figure 19: Variation in $\Theta(\eta)$ with P_r

tem gains more kinetic energy which enhances the velocity of the flow. The velocity in the x–direction reaches its peak at high Grashof number and low rotation parameter whereas the velocity in the z-direction reaches its peak at high Grashof number and high rotation. The result in Ref. [28] also agrees with this discovery. Fig. (22) shows that increase in buoyancy leads to a decrease in the temperature profile. The zoomed portion of Fig. (23) shows that the minimum temperature profile is reached at low rotation but high Grashof number. Temperature profiles decrease as buoyancy increases but an increase in rotation increases, alongside an increase in Grashof number, counters the effect of increasing Grashof number on the temperature profiles. The shear stress experiences a dual effect as the Grashof number increases. This is not shown for brevity but worth mentioning. As Grashof number increases, the shear stress reduces at the boundary layer but increases in the free stream. Increasing rotation alongside Grashof number magnifies the negative effect on shear stress both at the boundary layer and at the free stream. Hence, the minimum shear stress at the free stream is experienced at high rotation and high Grashof number. The result is in agreement with the results of Hussain *et al.* [34] and Koriko *et al.* [28].

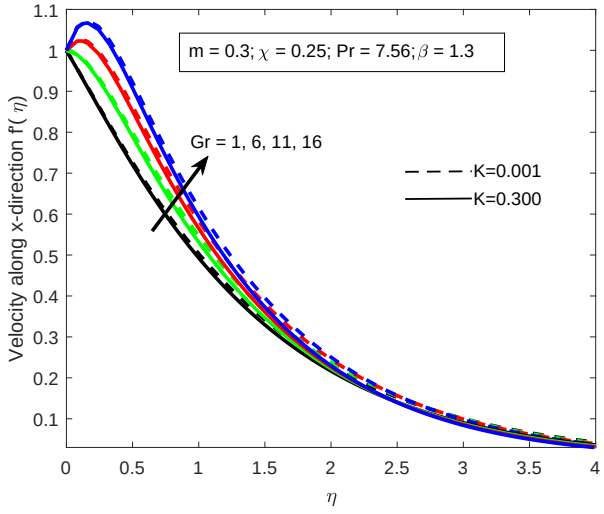

Figure 20: Variation of velocity profile in the x–direction with Grashof number

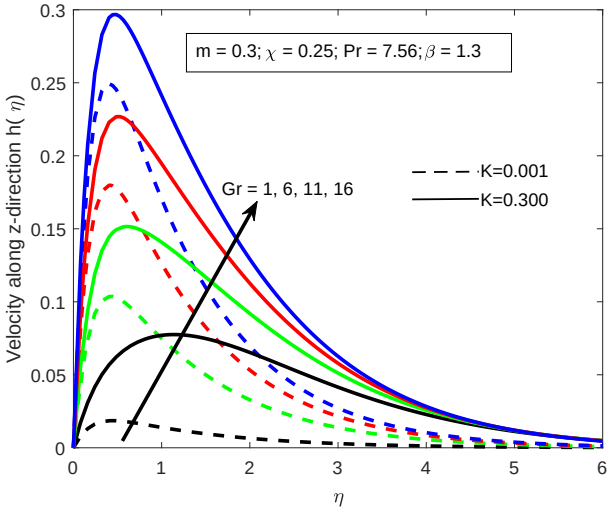

Figure 21: Variation of velocity profile in the z-direction with Grashof number

Table 3: Variation of quantities of interest with Casson fluid parameter $m = 0.3000$, $\chi = 0.1000$, $Gr = 3$, and $Pr = 1.3800$

β	K	C_{fx}	C_{fz}	N_{ux}	β	K	C_{fx}	C_{fz}	N_{ux}	β	K	C_{fx}	C_{fz}	N_{ux}
0.1	0.001	-0.108	0.1485	1.2547	0.1	0.2	-0.1118	0.1827	1.2537	0.1	0.3	-0.1152	0.1993	1.2528
0.4	0.001	-0.038	0.4421	1.2436	0.4	0.2	-0.0795	0.6376	1.2228	0.4	0.3	-0.0886	0.6606	1.2176
0.7	0.001	0.0279	0.6197	1.2421	0.7	0.2	-0.0191	0.8292	1.2209	0.7	0.3	-0.0323	0.8693	1.2145
1	0.001	0.0769	0.7393	1.242	1.0	0.2	0.0258	0.9652	1.2199	1	0.3	0.01	1.0136	1.2128
1.3	0.001	0.1139	0.8256	1.2422	1.3	0.2	0.0598	1.0646	1.2193	1.3	0.3	0.0421	1.1186	1.2118
1.6	0.001	0.1425	0.8908	1.2424	1.6	0.2	0.0862	1.1403	1.219	1.6	0.3	0.0671	1.1984	1.2112

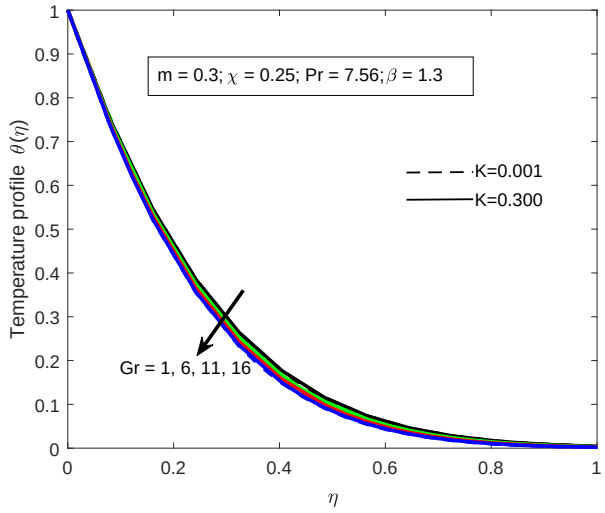

Figure 22: Variation of temperature profile with Grashof number

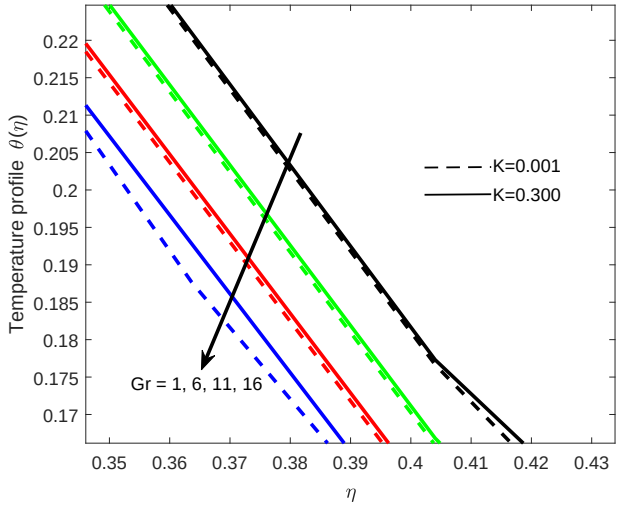

Figure 23: A zoomed portion of Fig.(22)

4.5 Quantities of interest

The quantities of interests are the Coefficient of Skin friction and heat transfer rate. It is observed from table (3) that at very low Coriolis force, increase in Casson fluid parameter causes at least 3.519% increase (at low β) and a maximum of 66.450% increase (at high β) in the coefficient of Skin Frictions but a dual effect on the heat transfer rate (increasing heat transfer rate when $\beta < 1$ but decreasing heat transfer rate when $\beta > 1$). Table (4) shows that at fixed rotation, the Prandtl number has negative effects on the coefficient of Skin Frictions in both directions (i.e. C_{fx} and C_{fz}) and significantly positive effect on heat transfer rate. As Coriolis force increases, simultaneously increasing Casson fluid parameter and Prandtl number reduces the skin friction coefficient in the x–direction and heat transfer rate but increases the skin friction coefficient in the z–direction. When all parameters are kept fixed, it can be seen from Table (5) that rotation has a reducing effect on the heat transfer rate and the Skin Friction in the x-direction but an increasing effect on the coefficient of Skin Friction in the z–direction. Using the slope linear regression through data points suggested in Shah *et al.* [35], Animasaun *et al.* [36], and Wakif *et al.* [37], it is seen that the local skin frictions in the flow along x–direction and heat transfer rate decrease with rotation parameter at the rate -0.0171 and -0.0037 respectively. However, local skin friction in the flow along$z$–direction increases with the rotation parameter at the rate of 0.1632.

5 Conclusion

The transport phenomenon of non-Newtonian Casson fluid over the upper horizontal rotating surface of a paraboloid of revolution had been analyzed. It is worth concluding that

- simultaneous increase in the Prandtl number, Casson fluid parameter, and Coriolis force has a negative effect on the velocity in the x–direction.
- simultaneous increase in Grashof number, Casson fluid parameter, and Coriolis force has an increasing effect on the velocity in the z–direction.
- simultaneous increase in the Prandtl number, Casson fluid parameter, and Coriolis force has a negative ef-

Table 4: Variation of quantities of interest with Grashof number $m = 0.3000$, $\chi = 0.2500$, $Gr = 3.00$, and $\beta = 0.1$

Pr	K	C_{fx}	C_{fz}	N_{ux}	Pr	K	C_{fx}	C_{fz}	N_{ux}
2	0.001	-0.1388	0.1192	1.6258	2	0.1	-0.1399	0.1359	1.6255
4	0.001	-0.1725	0.0830	2.4134	4	0.1	-0.1733	0.0995	2.4133
6	0.001	-0.1879	0.0666	3.0608	6	0.1	-0.1886	0.0831	3.0607
8	0.001	-0.1973	0.0568	3.6358	8	0.1	-0.1980	0.0733	3.6356
Pr	K	C_{fx}	C_{fz}	N_{ux}	Pr	K	C_{fx}	C_{fz}	N_{ux}
2	0.200	-0.1420	0.1527	1.625	2	0.3	-0.1451	0.1690	1.6242
4	0.200	-0.1751	0.1160	2.4128	4	0.3	-0.1780	0.1321	2.4121
6	0.200	-0.1904	0.0996	3.0603	6	0.3	-0.1932	0.1156	3.0597
8	0.200	-0.1997	0.0897	3.6352	8	0.3	-0.2024	0.1057	3.6346

Table 5: Variation of quantities of interest with rotation parameter $m = 0.3000$, $\chi = 0.2500$, $G = 3.0$, $Pr = 10$, and $\beta = 0.1$

K	C_{fx}	C_{fz}	N_{ux}
0.001	-0.2037	0.0501	4.1648
0.1	-0.2044	0.0666	4.1647
0.2	-0.2061	0.0829	4.1643
0.3	-0.2088	0.0989	4.1637

fect on shear stress in the boundary layer but an increasing effect on the shear stress at the free stream.

- simultaneous increase in both Casson fluid parameter and Coriolis force has an increasing effect on the temperature profile.
- At high rotation, Casson fluid parameter has a dual effect on the shear stress where the shear stress is positively favoured in the boundary layer but negatively affected in the free stream.
- Coriolis force causes an increase in the temperature and the velocity profile in the z–direction, a decrease in the velocity profile in the x–direction, and a dual effect on the shear stress.
- Coriolis force and the Casson fluid parameter have similar effects on the flow of Casson fluid over a rotating surface with non-uniform thickness.
- As Coriolis force increases, simultaneously increasing Casson fluid parameter and Prandtl number reduces the skin friction coefficient in the x–direction and heat transfer rate but increases the skin friction coefficient in the z–direction.
- When all parameters are kept fixed, the rotation has a reducing effect on the heat transfer rate and the Skin Friction in the x-direction but the increasing effect on the coefficient of Skin Friction in the z–direction.

It is important to mention here that at a very high rotation parameter, the flow becomes turbulent and a more devoted study will be required to study such flow.

Acknowledgements: All the authors deeply appreciate the suggestion and comments of the Reviewers and Editorial assistant.

Conflict of interest: The authors declare no conflict of interest regarding the publication of this paper.

References

[1] Debnath L. On Unsteady Magnetohydrodynamic Boundary Layers in a Rotating Flow. ZAMM - Zeitschrift fur Angewandte Mathematik und Mechanik;1972; 52(10):623 - 6. doi:10.1002/zamm.19720521010

[2] Deng L, Li T, Bi M, Liu J, Peng M. Dependence of tropical cyclone development on coriolis parameter: A theoretical model. Dynamics of Atmospheres and Oceans; 2018; 81: 51 - 62. doi:10.1016/j.dynatmoce.2017.12.001

[3] Archana M, Gireesha BJ, Prasannakumara BC, Gorla RSR. Influence of nonlinear thermal radiation on rotating flow of Casson nanofluid. Nonlinear Engineering; 2018; 7(2): 91 - 101. doi:10.1515/nleng-2017-0041

[4] Shiferaw AM, RamReddy C, Pradeepa T, Mathunjwa JS. Hall and ion-slip effects on mixed convection in a chemically reacting fluid between rotating and stationary disks. Nonlinear Engineering; 2018;7(1): 51 - 63. doi:10.1515/nleng-2017-0078

[5] Takhar HS, Chamkha AJ, Nath G. Unsteady mixed convection flow from a rotating vertical cone with a magnetic field. Heat and Mass Transfer; 2002; 39(4):297 - 304.doi:10.1007/s00231-002-0400-1

[6] Ghalambaz M, Behseresht A, Behseresht J, Chamkha A. Effects of nanoparticles diameter and concentration on natural convection of the Al_2O_3-water nanofluids considering variable thermal conductivity around a vertical cone in porous media. Advanced Powder Technology. 2015; 26(1):224-35.

[7] Makinde OD, Animasaun IL. Bioconvection in MHD nanofluid flow with nonlinear thermal radiation and quartic autocatalysis chemical reaction past an upper surface of a paraboloid of revolution. International Journal of Thermal Sciences. 2016; 109: 159-71.

Nomenclature

(x, y, z)	the spatial directions	$\boldsymbol{\Omega}$	angular velocity
(u, v, w)	dimensional velocity components in the (x, y, z) directions	μ	the plastic dynamic viscosity of the non-Newtonian fluid
m	velocity index	π	product of the component of deformation rate with itself
f_{bx}	body force in the $x-$ direction	π_c	critical value based on the non-Newtonian model
f_{bz}	body force in the $z-$ direction	e_{ij}	(i, j)th component of the deformation rate
g	acceleration due to gravity	μ	dynamic viscosity of Casson fluid
T	dimensional temperature	β	coefficient of expansion
T_∞	free stream temperature	β^*	Casson fluid parameter
T_w	temperature at the wall	c_p	heat capacity
h	dimensionless velocity in the $z-$ directions	κ	thermal conductivity
f'	dimensionless velocity in the $x-$ directions	ρ	density
K	rotational parameter	ψ	stream function
Pr	Prandtl number	θ	dimensionless temperature
Gr	Grashof number	η	similarity variable
C_{fx}	skin frictions along the $x-$direction	ϑ	kinematic viscosity
C_{fz}	skin frictions along the $z-$direction	χ	thickness parameter
N_{ux}	Nusselt number		

[8] Makinde OD, Animasaun IL. Thermophoresis and Brownian motion effects on MHD bioconvection of nanofluid with non-linear thermal radiation and quartic chemical reaction past an upper horizontal surface of a paraboloid of revolution. Journal of Molecular liquids. 2016; 221: 733-43.

[9] Animasaun IL. 47nm alumina-water nanofluid flow within boundary layer formed on upper horizontal surface of paraboloid of revolution in the presence of quartic autocatalysis chemical reaction. Alexandria Engineering Journal; 2016; 55(3):2375 - 89.doi: 10.1016/j.aej.2016.04.030

[10] Animasaun IL. Significance of quartic autocatalysis on fluid flows conveying nanoparticles, dust-particles and microstructures over an object with non-uniform thickness. Ph.D. Thesis Submitted to The Federal University of Technology Akure, Nigeria; 2019.

[11] Liu H, Animasaun IL, Shah NA, Koriko OK, Mahanthesh B. Further discussion on the significance of quartic autocatalysis on the dynamics of water conveying 47 nm alumina and 29 nm cupric nanoparticles. Arabian Journal for Science and Engineering. 2020; 45(7):5977-6004.

[12] Koriko OK, Animasaun IL, Mahanthesh B, Saleem S, Sarojamma G, Sivaraj R. Heat transfer in the flow of blood-gold Carreau nanofluid induced by partial slip and buoyancy. Heat Transfer-Asian Research. 2018; 47(6):806-23.

[13] Makinde OD, Omojola MT, Mahanthesh B, Alao FI, Adegbie KS, Animasaun IL, Wakif A, Sivaraj R, Tshehla MS. Significance of buoyancy, velocity index and thickness of an upper horizontal surface of a paraboloid of revolution: The case of non-Newtonian Carreau fluid. InDefect and Diffusion Forum 2018; 387; 550-561).

[14] Ajayi TM, Omowaye AJ, Animasaun IL. Viscous dissipation effects on the motion of Casson fluid over an upper horizontal thermally stratified melting surface of a paraboloid of revolution: boundary layer analysis. Journal of Applied Mathematics. 2017; Article ID 1697135.

[15] RamReddy C, Surender O, Rao CV. Effects of Soret, Hall and Ion-slip on mixed convection in an electrically conducting Casson fluid in a vertical channel. Nonlinear Engineering. 2016; 5(3):167-75.

[16] Amanulla CH, Nagendra N, Reddy MS. Computational analysis of non-Newtonian boundary layer flow of nanofluid past a semi-infinite vertical plate with partial slip. Nonlinear Engineering. 2018; 7(1):29-43.

[17] Batra RL, Jena B. Flow of a Casson fluid in a slightly curved tube. International journal of engineering science. 1991 Jan 1;29(10):1245-58.

[18] Siddiqui SU, Verma NK, Mishra S, Gupta RS. Mathematical modelling of pulsatile flow of Casson's fluid in arterial stenosis. Applied Mathematics and Computation. 2009; 210(1):1-0.

[19] Abegunrin OA, Okhuevbie SO, Animasaun IL. Comparison between the flow of two non-Newtonian fluids over an upper horizontal surface of paraboloid of revolution: Boundary layer analysis. Alexandria Engineering Journal. 2016;55(3):1915-29.

[20] Sankar DS, Lee U. Two-fluid Casson model for pulsatile blood flow through stenosed arteries: A theoretical model. Communications in Nonlinear Science and Numerical Simulation. 2010; 15(8): 2086-97.

[21] Mukhopadhyay S, De PR, Bhattacharyya K, Layek GC. Casson fluid flow over an unsteady stretching surface. Ain Shams Engineering Journal. 2013; 4(4):933-8.

[22] Pramanik S. Casson fluid flow and heat transfer past an exponentially porous stretching surface in presence of thermal radiation. Ain Shams Engineering Journal. 2014 Mar 1;5(1):205-12.

[23] Animasaun IL. Effects of thermophoresis, variable viscosity and thermal conductivity on free convective heat and mass transfer of non-Darcian MHD dissipative Casson fluid flow with suction and nth order of chemical reaction. Journal of the Nigerian Mathematical Society. 2015; 34(1):11-31.

[24] Kataria HR, Patel HR. Radiation and chemical reaction effects on MHD Casson fluid flow past an oscillating vertical plate embedded in porous medium. Alexandria Engineering Journal. 2016; 55(1): 583-95.

[25] Zaib A, Bhattacharyya K, Uddin M, Shafie S. Dual solutions of non-Newtonian Casson fluid flow and heat transfer over an exponentially permeable shrinking sheet with viscous dissipation. Modelling and Simulation in Engineering. 2016; 2016.
[26] Abbasian M, Shams M, Valizadeh Z, Moshfegh A, Javadzadegan A, Cheng S. Effects of different non-Newtonian models on unsteady blood flow hemodynamics in patient-specific arterial models with in-vivo validation. Computer methods and programs in biomedicine. 2020; 186:105185.
[27] Dubey A, Vasu B, Anwar Beg O, Gorla RS, Kadir A. Computational fluid dynamic simulation of two-fluid non-Newtonian nanohemodynamics through a diseased artery with a stenosis and aneurysm. Computer Methods in Biomechanics and Biomedical Engineering. 2020:1-27.
[28] Koriko OK, Adegbie KS, Oke AS, Animasaun IL. Exploration of Coriolis force on motion of air over the upper horizontal surface of a paraboloid of revolution. Physica Scripta. 2020; 95(3):035210.
[29] Mustafa M, Hayat T, Pop I, Aziz A. Unsteady boundary layer flow of a Casson fluid due to an impulsively started moving flat plate. Heat Transfer-Asian Research. 2011;40(6):563-76.
[30] Oke AS. Convergence of differential transform method for ordinary differential equations. Journal of Advances in Mathematics and Computer Science. 2017 Oct 10:1 - 7.
[31] Malik MY, Khan M, Salahuddin T, Khan I. Variable viscosity and MHD flow in Casson fluid with Cattaneo-Christov heat flux model: Using Keller box method. Engineering Science and Technology, an International Journal. 2016 Dec 1;19(4):1985-92.
[32] Patel HR. Effects of cross diffusion and heat generation on mixed convective MHD flow of Casson fluid through porous medium with non-linear thermal radiation. Heliyon. 2019 Apr 1;5(4):e01555.
[33] Animasaun IL, Adebile EA, Fagbade AI. Casson fluid flow with variable thermo-physical property along exponentially stretching sheet with suction and exponentially decaying internal heat generation using the homotopy analysis method. Journal of the Nigerian Mathematical Society. 2016;35(1):1-7.
[34] Hussain SM, Jain J, Seth GS, Rashidi MM. Free convective heat transfer with hall effects, heat absorption and chemical reaction over an accelerated moving plate in a rotating system. Journal of Magnetism and Magnetic Materials. 2017;422:112-23.
[35] Shah NA, Animasaun IL, Ibraheem RO, Babatunde HA, Sandeep N, Pop I. Scrutinization of the effects of Grashof number on the flow of different fluids driven by convection over various surfaces. Journal of Molecular liquids. 2018; 249:980-90.
[36] Animasaun IL, Ibraheem RO, Mahanthesh B, Babatunde HA. A meta-analysis on the effects of haphazard motion of tiny/nano-sized particles on the dynamics and other physical properties of some fluids. Chinese Journal of Physics. 2019 Aug 1;60:676-87.
[37] Wakif, A., Animasaun, I. L., Satya Narayana, P. V., & Sarojamma, G. (2019). Meta-analysis on thermo-migration of tiny/nano-sized particles in the motion of various fluids. Chinese Journal of Physics, in-press. doi:10.1016/j.cjph.2019.12.002